Sensors and Actuators B 220 (2015) 50–58

Contents lists available at ScienceDirect

Sensors and Actuators B: Chemical

journal homepage: www.elsevier.com/locate/snb

Synthesis and characterization of $MnFe_2O_4$ nanoparticles for impedometric ammonia gas sensor

Ramasamy Hari Vignesh[a,b], Kalimuthu Vijaya Sankar[a], Samuthirapandian Amaresh[b], Yun Sung Lee[b,*], Ramakrishnan Kalai Selvan[a,*]

[a] Solid State Ionics and Energy Devices Laboratory, Department of Physics, Bharathiar University, Coimbatore 641 046, Tamil Nadu, India
[b] Faculty of Applied Chemical Engineering, Chonnam National University, Gwangju 500-757, Republic of Korea

ARTICLE INFO

Article history:
Received 28 October 2014
Received in revised form 1 April 2015
Accepted 10 April 2015
Available online 19 May 2015

Keywords:
Spinel structure
Metal oxides
Tetra ethylene glycol
Impedemetric gas sensor
Barrier height

ABSTRACT

Growing concentration of toxic gases in the atmosphere presents a great challenge in the identification of suitable and novel gas sensing materials, with good selectivity at room temperature. This work demonstrates a facile synthesis of $MnFe_2O_4$ nanoparticles by solution assisted combustion synthesis. The synthesized materials are characterized by XRD, FTIR, FE-SEM to confirm the crystal structure and surface morphology. The ferromagnetic behavior of prepared $MnFe_2O_4$ at room temperature was revealed through VSM analysis. The N_2 adsorption–desorption isotherm and BET surface area analysis confirms the mesoporous nature with the surface area of 33 $m^2\ g^{-1}$. The room temperature sensing behavior of $MnFe_2O_4$ is studied using impedometric technique for analyzing ammonia gas. The prepared $MnFe_2O_4$ is robust and shows a sensitivity of 100% for increasing concentration of ammonia vapor. The conductivity increased in the order of 10^2 magnitudes while increasing ammonia concentration. It shows the high selectivity of 83.5% for 10 ppm towards ammonia over other toxic gases like chloroform, etc. The room temperature (303 K) operation, with high sensitivity, selectivity, together with the low cost suggests suitability of developing a new, high power cost-effective ammonia sensor.

1. Introduction

The air that we breathe includes different chemical species, some of which being advantage, while others are hazardous. The rapid development of human population along with civilization requires cheaper and reliable methods of measuring the concentrations of the toxic, biological and greenhouse gases. Recently, many sensors have been utilized which works on various principles and materials [1,2]. A chemical gas sensor can be defined as the device which upon exposure to the gas species or molecules alters one or more of its physical properties such as mass, electrical conductivity and dielectric property in a way that is possible to measure and quantify. These changes deliver an electrical signal that is proportional to the concentration of the gas under test. The sensitivity of the particular gas depends on the material used. The sensors find applications in many important areas, namely environmental monitoring, domestic safety, public security, automobile applications, etc. [3]. Several analytical techniques to detect ammonia in gas/vapor/liquid stream include the electrochemical method [4], laser technology [5], mass spectrometry [6] and optical method [7]. These techniques were found to be time consuming and required sophisticated instruments. Hence a cheap and practical ammonia sensor would be preferable to our day-to-day applications. Transition metal oxides are capable as a gas sensing element because of its strong atmosphere dependent electrical conduction. Ammonia is a highly toxic gas existing in air, soil and water. Ammonia is produced in many chemical and biological industries, fertilizer factories, refrigeration systems, food processing and medical diagnosis. On the other hand ammonia is produced by the human body, which makes the ammonia analyzers useful for the diagnosis of certain diseases [8]. Despite all these facts, even a small leakage of ammonia can cause huge damage to human health [2]. Occupational Safety and Health Administration (OSHA) established the maximum recommended exposure level of ammonia to be 25 ppm beyond which may cause eye irritation, skin ailments, vomiting, etc. [9]. Due to this the development of a highly sensitive ammonia sensor is an active area of research.

One of the first report for ammonia gas sensor was based on the decrease in the conductance of the conducting polypyrrole on exposure to ammonia gas [10]. So far NH_3 sensors were prepared using various sensing materials such as SnO_2 [11], TiO_2 [12], MoO_3 [13],

* Corresponding authors.
E-mail addresses: leeys@chonnam.ac.kr (Y.S. Lee), selvankram@buc.edu.in (R.K. Selvan).

http://dx.doi.org/10.1016/j.snb.2015.04.115
0925-4005/

V_2O_5 [14], In_2O_3 [15], conducting polymers [12], reduced graphene oxide [16], etc. Among these, transition metal oxides is one of the alternative class of inorganic solids for ammonia sensors, due to its variety of crystallographic structures, properties, low cost, strong stability in chemical and thermal atmosphere [3]. This creates a great demand for novel materials as sensors with highly improved properties. Spinel's of the type $M^{2+}M_2{}^{3+}O_4$ attract the research interest because of their versatile practical applications. In case of M^{3+} = Fe the resulting spinel ferrites having a general chemical composition of MFe_2O_4 (M = Mn, Mg, Zn, Co, Cd, etc.) is widely used as magnetic materials. Presently, this is a topic of increasing interest to study the gas sensing properties of ferrites. Particularly gas sensing at room temperature is of great interest [17]. Here $MnFe_2O_4$ is being used as the sensing material because of its multiple valence states of Mn and eco-friendly properties. To the best of our knowledge for the first time $MnFe_2O_4$ is being used as the ammonia sensing material.

The sensitivity of the material depends on its microstructural properties along with its method of preparation. The later plays a very important role in determining the chemical and structural properties of a spinel ferrite [18]. Different methods are available for the synthesis of nanosized magnetic spinel ferrite $MnFe_2O_4$ nanoparticles, such as co-precipitation [19], hydrothermal method [20], solid state reaction [21], thermal decomposition [22], solvothermal method [23], etc. However, there is no report available for the synthesis of $MnFe_2O_4$ nanoparticles by tetra ethylene glycol [TEG] assisted combustion method. This method is cost effective, single step easy method to obtain metal oxides with high phase purity, crystallinity, particle homogeneity and surface area [24]. $MnFe_2O_4$ is tested as novel materials for gas sensing applications, particularly for toxic gas like ammonia, which have major roles in our day to day life. The main purpose of this research is to find the electrical properties as well as to explore $MnFe_2O_4$ as an ammonia detecting element. The conductivity is found to vary in the order of magnitude of 10^2 with varying concentration of ammonia. It exhibits good sensitivity for the toxic NH_3 gas.

2. Materials and methods

2.1. Synthesis of $MnFe_2O_4$ nanoparticles

The materials used in the preparation are $Mn(NO_3)_2{\cdot}4H_2O$, $Fe(NO_3)_2{\cdot}9H_2O$, and glycine. For the typical synthesis, the stochiometric quantities of $Mn(NO_3)_2{\cdot}4H_2O$ (1.633 g), $Fe(NO_3)_2{\cdot}9H_2O$ (5.255 g) and of glycine (0.488 g) are dissolved in 2, 3, and 10 mL of distilled water separately. All the solutions are simultaneously poured into the desired amount of tetra ethylene glycol (TEG) contained quartz crucible. Then the mixed precursor solution is heated at 80 °C for the dehydration reaction. Subsequently, the obtained dried gel is kept at electric heater and maintained the temperature of around 300 °C for igniting combustion reaction. Once the combustion reaction started, the fire starts from the surface and extends to the interior. After completion, the obtained foamy black powder was ground well using mortar and pestle. It was stored for further characterization without any high temperature calcination.

2.2. Material characterization

Phase formation and morphology analysis was carried out using the powder diffractometer 5635 (Siemens D500 advance) with CuKα radiation and high magnification with a field emission scanning electron microscopy (FESEM) on a Zeiss Ultra FEG 55 instrument at 20 kV operating voltage. Bruker Tensor 27 FT-IR Instrument is used for FTIR Studies. Magnetic properties were measured using the VSM (Lakeshore, USA; Model 7404). The surface area, pore size, pore distribution of the samples are determined using the nitrogen adsorption–desorption experiment at 77 K (micrometrics ASAP 2010 surface area analyzer) and calibrated by the BET and BJH method respectively. The conductivity change of the sample in gas atmosphere was analyzed using an LCR meter (HIOKI 3532 LCR).

2.3. Sensor fabrication and measurements

Ammonia sensor is fabricated using a thin pressed pellet of MnFe2O4 nanoparticles (600 mg). The pellet was affixed in between two stainless steel electrodes and the whole setup was placed in a glass chamber of volume 150 mL for sensing the ammonia gas. The set up was left in the air until a steady baseline resistance was reached and then measurements are made in ammonia atmosphere. The gas sensing experiments were conducted at room temperature. The volume of ammonia (V) required to achieve the specific vapor concentration in ppm inside the test chamber was obtained using Eq. (1) [24].

$$V = \frac{CV_aM}{\left(2.46 \times 10^7\right) \times D} \quad (1)$$

where C is the concentration of sensing gas (ppm), V is the required liquid volume (μL), D is the density of ammonia (g m μL^{-1}), V_a is the volume of air which is equal to the volume of test chamber (mL) and M is the molecular weight of ammonia (g mol^{-1}). The sensing behavior was studied by injecting the desired amount of ammonia into the glass chamber. Measurements were made at suitable intervals of time.

3. Results and discussion

3.1. Structural and morphological properties

Fig. 1(a) shows the XRD pattern of $MnFe_2O_4$ nanoparticles. The high intensity and well defined peaks infers the good crystallinity of the $MnFe_2O_4$ nanoparticles. The observed diffraction peaks at 30.10°, 35.42°, 43.10°, 53.72°, 56.94° and 62.46° corresponds to the lattice planes of (2 2 0), (3 1 1), (4 0 0), (5 1 1), (4 4 0) and (4 4 4), respectively. It is well concord with standard JCPDS (No. 10-0319). No other oxide (Fe_2O_3) or impurity peaks were observed which infers the phase purity of the $MnFe_2O_4$. In addition, the calculated lattice constant of 8.420 Å reveals the cubic structure of $MnFe_2O_4$. The calculated lattice density and lattice volume is 5.12 g cm^{-3} and 597 Å^3, respectively, which are well agreed with standard values. Using Scherrer's equation [25], the calculated grain size is 20 nm for the high intensity (3 1 1) plane. This smaller grain size, enhances the surface free energy which in turn helps in more adsorption of gas molecules on the surface. The FT-IR spectrum (Fig. 1(b)) shows the two characteristic vibration bands of $MnFe_2O_4$ located at around 576 and 389 cm^{-1} corresponds to the vibrational modes of tetrahedral and octahedral sites [26], respectively. No other metal oxide bands are identified between 400 and 1000 cm^{-1}, which further confirms the single phase formation of $MnFe_2O_4$. The FE-SEM image (Fig. 1(c)) evidenced that the particles are having almost spherical like morphology. Using SCION image software the average particles size was found to be in the range of 30–35 nm. In addition, the partial aggregation is also observed. This mixed rough and granular morphology helps in the conductivity applications of high electron transfer. As well as the smaller sized nanoparticles improves the specific surface area, which enhances the adsorption of gaseous molecules on the surface of the sample thereby increasing the conductivity.

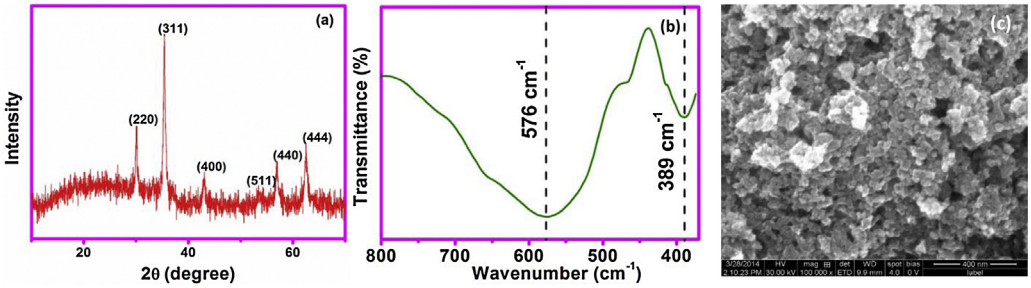

Fig. 1. (a) XRD, (b) FT-IR spectrum and (c) FE-SEM image of $MnFe_2O_4$ nanoparticles.

3.2. Magnetic properties

In order to identify the field dependent magnetic properties of the $MnFe_2O_4$ nanoparticles, the VSM analysis is carried out and is given in Fig. S1. The obtained hysteresis loop shows that $MnFe_2O_4$ is a soft ferrite and having ferromagnetic behavior. The saturation magnetization (M_S) is found to be 46 emu/g, which is lower than the bulk counterpart (80 emu/g) and comparable with the reported values [27–29]. This lower saturation magnetization may be attributed to several reasons such as particle size, crystalline nature, arrangement of particles, as well as the adsorbed layer of molecules on the particle surface, the existence of random canting of particle surface spins [30–32]. In addition, it also depends upon the concentration of divalent and trivalent cations in the octahedral and tetrahedral sites, respectively [33]. Similarly, for the nanosized particles, the surface to volume ratio is high, which decreases the saturation magnetization [34]. The obtained coercivity is low, *i.e.*, 64 G indicating that all of them accorded with properties of soft magnetic material. Coercivity represents the strength of the magnetic field necessary to overcome the anisotropy barrier and allow magnetization of the nanoparticles following the magnetic field orientation.

3.3. Surface area analysis

Fig. 2(a and b) shows the N_2 adsorpsion–desorpsion isotherm and pore size distribution curve of $MnFe_2O_4$ nanoparticles. It is found that the adsorption–desorption isotherm belongs to type III isotherm in the Brunauer classification [35]. Absence of micropores can be identified by the fact that there is no steep increase in the isotherm at low relative pressure. The gradual increase in the low relative pressure region shows the presence of developed mesopores with narrow pore size distribution. Vertical tail at the high pressure region indicates the presence of macro pores. The presence of slit like and the ink-bottle type pores are known by the H3 hysteresis at the high pressure region. According to the Kelvin equation the ink-bottle type pores possesses larger pore size in the bottle body which gives hysteresis in the high relative pressure region [36,37]. The total specific surface area (SSA) is estimated using the Brunauer–Emmett–Teller (BET) and is found to be 33.479 $m^2\ g^{-1}$ with total pore volume of 0.1609 $cm^3\ g^{-1}$. The average pore diameter is 19.23 nm. The pore size distribution which is particularly important for many pore size dependent applications was calculated using the Barrett–Joyner–Halenda (BJH theory). It is found that the majority of the pores are found to be in the region of 10–50 nm range with the peak at 28.07 nm indicating the mesoporous nature.

3.4. Impedimetric gas sensor

The AC impedimetric study is suitable and non-destructive method for analyzing the electrical process taking place in the material. It is a useful tool to study defects, electrical conductivity and the surface chemistry of materials including dielectrics, ionic conductors, aqueous solutions and the adsorbate–adsorbent interfaces [38,39]. It is well known that the AC impedimetric plot consists of single or double semicircles which depend on the conduction mechanism. The appearance of single semicircle at high frequency region represents the bulk conduction of the materials. Subsequently, the semicircle appeared at low frequency region indicates the role of grain boundary conduction in electrical process [40] Based on the above mentioned concept, for the first time the NH_3 gas sensing behavior of $MnFe_2O_4$ nanoparticles is studied over a wide range of concentrations from 10 to 1000 ppm. Fig. 3(a–e) shows the impedance spectra of the $MnFe_2O_4$ nanoparticle measured at room temperature under various concentrations of ammonia. It is observed that the gradual evolution of the semicircular arc at high frequency due to the effect of gas concentration. The similar type of observations has already been reported for α-Fe_2O_3 compound [24].

This semicircle helps in visualizing the equivalent circuit for electrical process occurring within the materials and their correlation with the micro structural properties. The bulk resistance

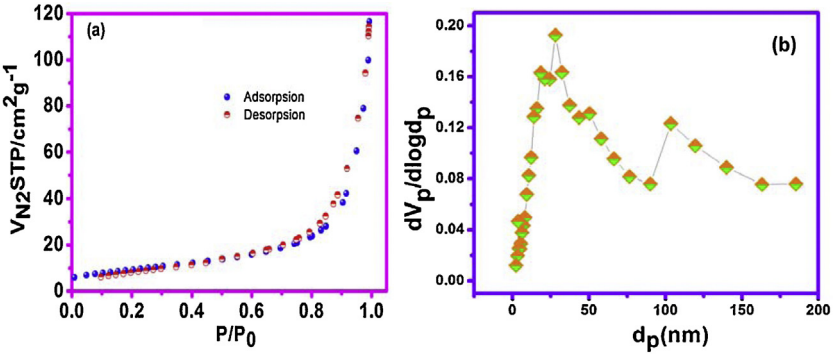

Fig. 2. (a) N_2 adsorption–desorption isotherm and (b) BJH curve of $MnFe_2O_4$ nanoparticles.

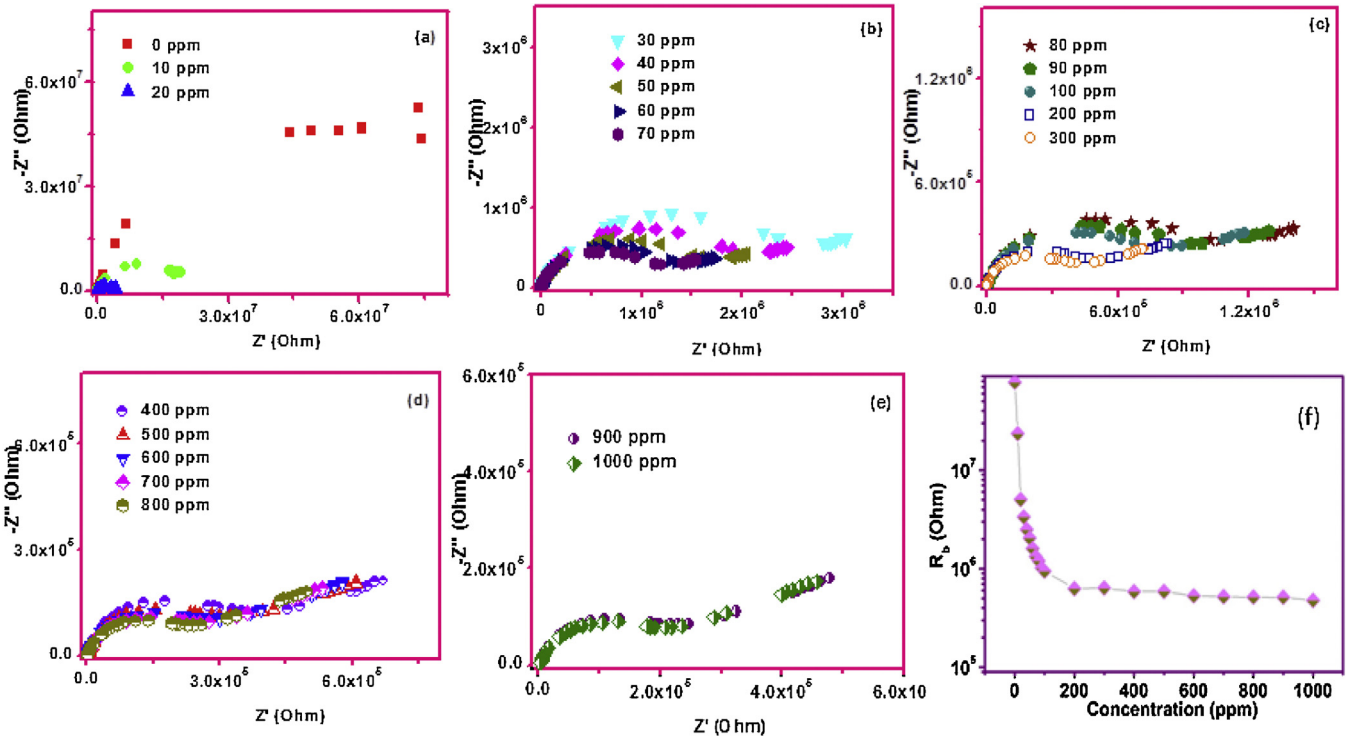

Fig. 3. (a-e) Cole-Cole plot of $MnFe_2O_4$ at different ammonia concentrations (10–1000 ppm) and (f) Variation of bulk resistances with concentration of NH_3.

(R_b) is found by extrapolating the semicircle and finding its intercepts on the real axis (Z') at low frequency region. This gives the useful information about the electrical properties of the system. Each semicircle can be represented as the parallel combination of capacitance and resistance [41]. A single semi-circle arc is observed when the concentration of ammonia is less than 30 ppm (Fig. 3(a)) and the intersection on the real axis is shifted towards the lower frequency region. It reveals the decrease of resistance or increase of conductivity with respect to gas concentration. While further increasing the concentration from 40 to 1000 ppm (Fig. 3(b–e)), the second semi-circular arc starts to appear, which indicates the existence of both bulk and grain boundary conductivity [40]. Fig. 3(f) shows the obtained bulk resistance (R_b) of $MnFe_2O_4$ at different concentrations of ammonia. Huge decrease of R_b with increasing concentration of ammonia reveals the good sensitivity of $MnFe_2O_4$. The conductivity is calculated using the following equation (Eq. (2)), and found to increase with increase in the ammonia concentration.

$$\sigma = \frac{l}{AR_b} \tag{2}$$

where 'l' is the thickness of the sample, R_b is the resistance obtained from the plot and A is the area of the pellet (πr^2). The maximum obtained (Fig. S2) conductivity is 8.177×10^{-5} S cm^{-1} at 1000 ppm, which is approximately 10^2-fold higher than conductivity of $MnFe_2O_4$ in the absence of NH_3 atmosphere (4.98×10^{-7} S cm^{-1}). It reveals the good NH_3 sensing behavior of $MnFe_2O_4$ even at lower concentration of 10 ppm. Further, the effect of NH_3 concentration on the bulk capacitance is calculated using the equation (Eq. (3))

$$C_b = \frac{1}{2\pi R_b \gamma_{max}} \tag{3}$$

where C_b is bulk capacitance, R_b is bulk resistance, γ_{max} is maximum frequency. The calculated capacitance is in the range of 10–5 pF. It was clearly seen from the above equation that the capacitance was inversely proportional to the frequency. The higher capacitance at lower frequency was due to the fact that at lower frequency the charge carriers have the time to follow the changes in the electric field. Under this condition the response of the sensor is largely affected by the NH_3 gas. At higher frequencies the change of electric field becomes very fast that it becomes difficult for the charge carriers to adjust to it [42], which enumerates the variation of bulk capacitance with respect to NH_3 concentration.

Under the application of the ac field, frequency dispersion or dielectric relaxation is observed due to a number of polarization mechanisms. Each relaxation process was characterized by the relaxation time which describes the decay of polarization with time in the periodic field. These relaxation time can be calculated from (a) loss spectrum or (b) Nyquist plot, which convey the same meaning [39,44]. This relaxation process gives raise to the unique relaxation frequency in the Nyquist plot. The variation of the relaxation frequency and relaxation time with respect to ammonia concentration are given in Fig. 4(a). It evidenced that the concentration of ammonia greatly alters the relaxation frequency. Subsequently, the bulk relaxation time is calculated using the following equation

$$\tau = \frac{1}{2\pi f_{max}} \tag{4}$$

where, f_{max} is the relaxation frequency obtained from the Nyquist plot [43]. The calculated relaxation time at 1000 ppm is 10^2 times lesser than the relaxation time at 0 ppm. This shows that more electrical properties are taking place within the material due to migration of the immobile species/defects. All these data is found to be in great agreement with the above results. The decrease of resistivity in two orders of magnitude shows that $MnFe_2O_4$ is suitable for sensing ammonia gas.

Fig. 4(b–f) shows relation between the imaginary part of impedance and frequency of $MnFe_2O_4$ in different NH_3 concentration. This spectra provides the useful information about the relaxation process of the $MnFe_2O_4$ in the presence of NH_3 gas. It can be seen that upto 20 ppm (Fig. 4(b)), there is no evidence for

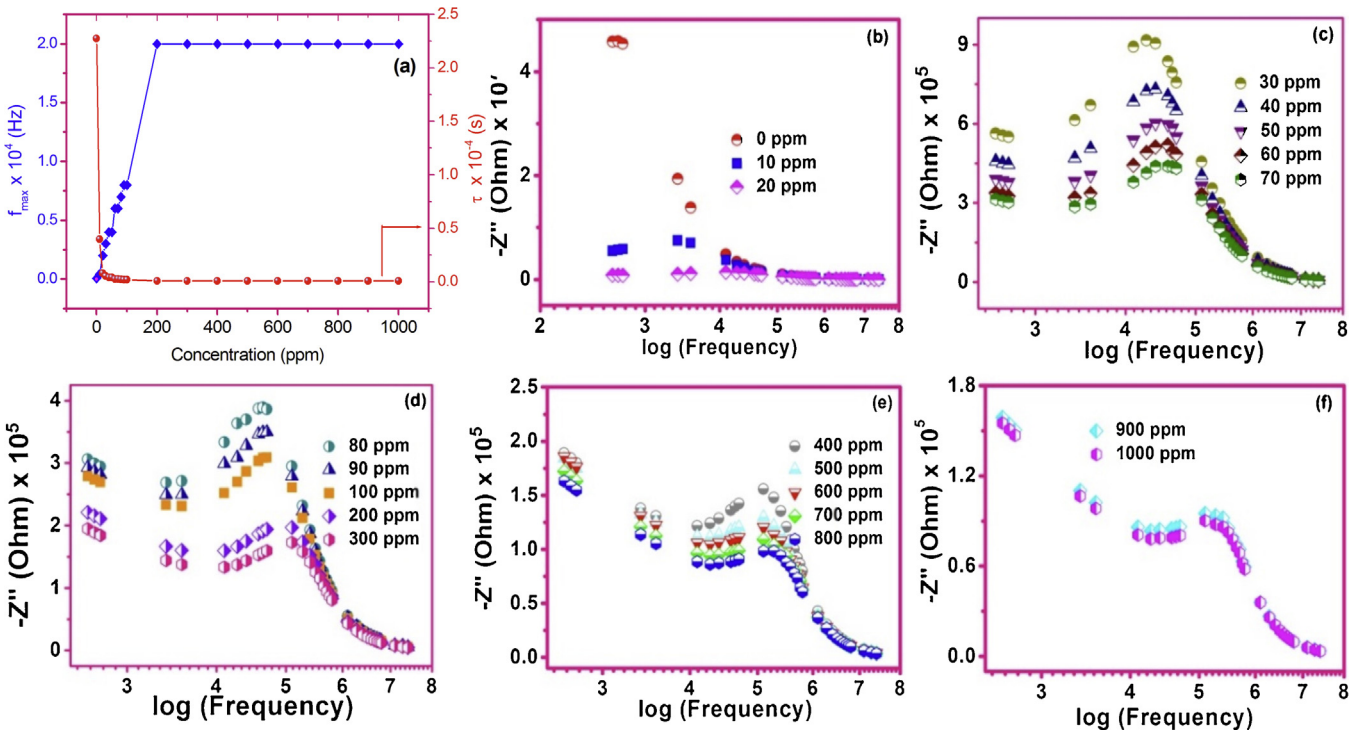

Fig. 4. (a) Variation of relaxation frequency (f_{max}) and relaxation time (τ) with NH_3 concentration and (b-f) loss spectra of $MnFe_2O_4$ at different NH_3 concentration.

the formation of relaxation peak. It indicates that the nil possibility of relaxation process in the measured frequency range. On the other hand, at higher concentration of NH_3 (Fig. 4(c–f)), the presence of peak broadening and peak shifting is noticed, which indicates the occurrence of concentration dependant relaxation process in $MnFe_2O_4$. There is an asymmetric peak broadening which suggests the process of electrical phenomenon in the material with the spread of the relaxation time. In general, the electrical relaxation process is carried out by the presence of electrons/immobile species [44,45]. Finally, the concentration dependent relaxation process concludes that $MnFe_2O_4$ is suitable material for sensing NH_3 even at low concentration of 10 ppm.

3.5. Sensing mechanism of $MnFe_2O_4$ nanoparticles

It is familiar that the surface controlled mechanism is responsible for sensing mechanism in the metal oxide based gas sensors [46]. The NH_3 gas sensing mechanism of $MnFe_2O_4$ nanoparticles is schematically represented in Fig. 5 at various stages. In stage 1, more free electrons are presented in the conduction band of $MnFe_2O_4$. The atmospheric oxygen molecules (O_2) are adsorbed on the surface of the pellet (Stage 2), while exposing the $MnFe_2O_4$ pellet in to air atmosphere. Here, the electrons from the conduction band are captured by these adsorbed oxygen, making $MnFe_2O_4$ to have many surface adsorbed oxygen ion species like O^-, and O^{2-}, where O^{2-} forms the majority of the adsorbed species. These ions play a vital role in the gas sensing process [24]. Further, the electrical properties of the $MnFe_2O_4$ nanoparticles are tuned, as the gas adsorbs on the broken or weakened bond on the surface, which act as the active sites for gas adsorption. A depletion layer is formed at the surface of the individual particles and inter-granular regions when the electrons in the conduction band are restricted in their motion by the oxygen species. This is the rate determining step for the sensing mechanism. The surface resistance reaches a stabilized value when the chemisorpsion of oxygen at the surface attains equilibrium, forming the baseline resistance for the calculation of sensitivity (resistance in the presence of air) [47]. Here the mesoporous nature of $MnFe_2O_4$ would help in the effective gas diffusion and adsorption by increasing the inner and outer surface area. This causes more oxygen species get adsorbed on the material surface [stage 2]. The ionization of the oxygen can be expressed as [48–50]

$$O_{2(gas)} = O_{2(ads)} \quad (5)$$

$$O_{2(ads)} + e^- = {O_{2(ads)}}^- \quad (6)$$

$${O_{2(ads)}}^- + e^- = 2{O_{(ads)}}^- \quad (7)$$

$${O_{(ads)}}^- + e^- = {O_{(ads)}}^{2-} \quad (8)$$

where the subscripts 'gas' and 'ads' indicates the gaseous and adsorbed oxygen [51]. Upon exposure to reducing gases like ammonia, these molecules get oxidized with the adsorbed oxygen ions, by following a series of intermediate stages, producing NO and H_2O molecules. The resulting O atoms in non-lattice positions are more likely to attract the H atoms from neighboring NH_3 molecules, and as a result water formation takes place. The energy released during the decomposition of ammonia molecule would be sufficient for the trapped electrons to jump into the conduction band of $MnFe_2O_4$ resulting in an increase in the conductivity of pellet of $MnFe_2O_4$ [stage 3]. This shows n-type conduction mechanism which is similar to other metal oxide semiconductors reported in the literature [52,53]. The best response is produced with a large amount of ammonia gas favoring the reaction between the adsorbed reducing gas and the oxygen species [stage 4]. Three types of reactions are proposed for ammonia oxidation on metal oxides [24,54].

$$2NH_3 + 3(O) = 3H_2O + 6e^- \quad (9)$$

$$2NH_3 + 4(O) = N_2O + 3H_2O + 8e^- \quad (10)$$

$$2NH_3 + 5(O) = 2NO + 3H_2O + 10e^- \quad (11)$$

The symbol O denotes the oxides in regular oxygen sites and it can be substituted by appropriate amounts of chemisorbed

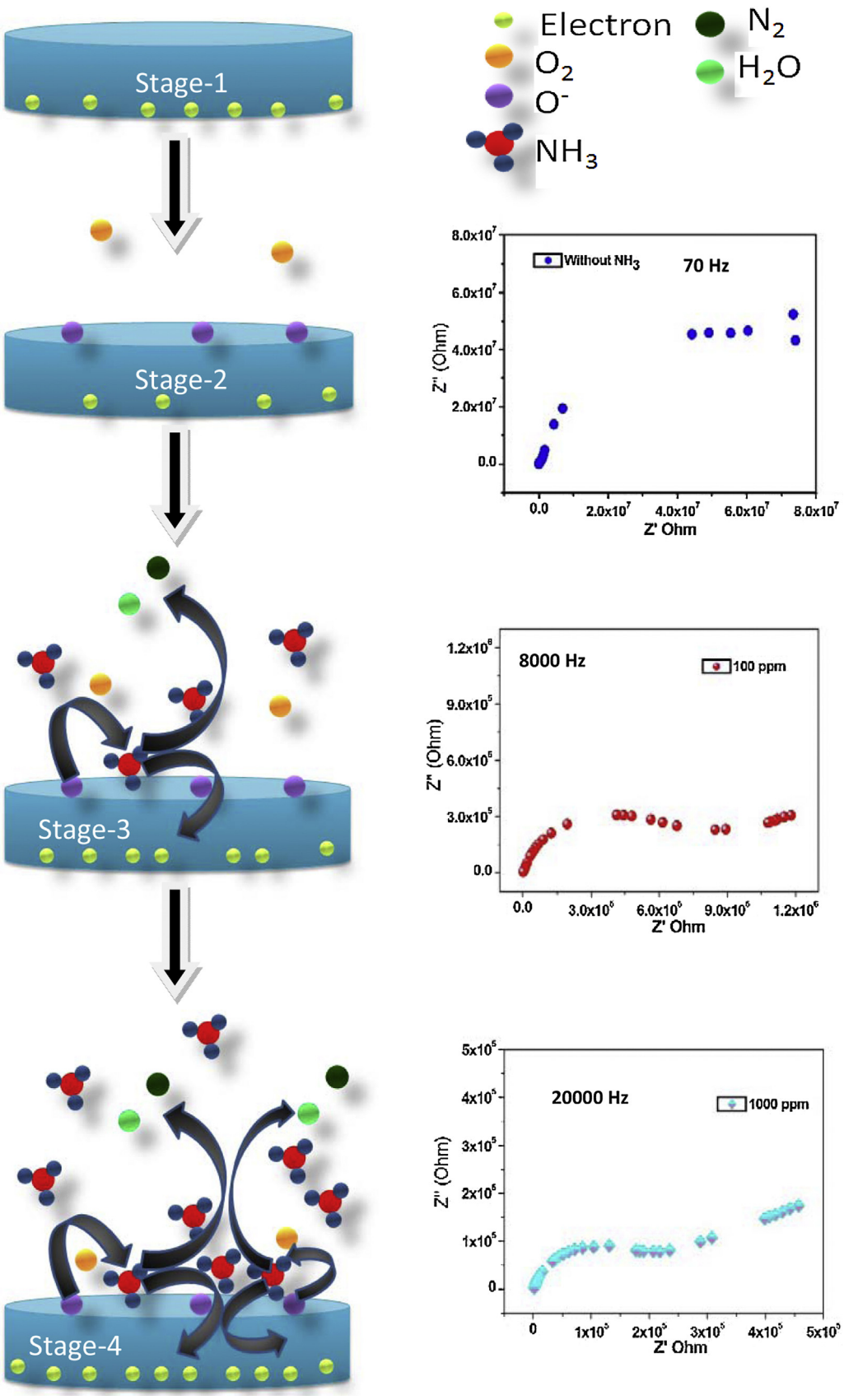

Fig. 5. Schematic representations for the conduction mechanism of $MnFe_2O_4$ in NH_3 atmosphere.

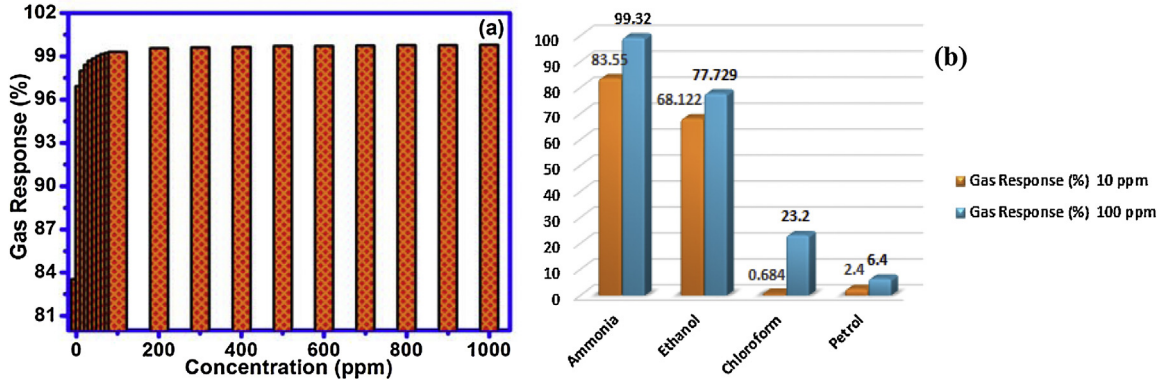

Fig. 6. (a) Variation of gas response with NH_3 concentration and (b) gas response of $MnFe_2O_4$ in various gases.

O_2^- and O^- species. The significance of this observation is in the very low detection of ammonia at room temperature.

3.6. Effect of NH_3 concentration on barrier height

The variation of conductivity with frequency is represented in the conduction spectra (Fig. S3). It consists of two regions such as d.c. region and a.c. region. The frequency independent conductivity region is called d.c. region. Similarly the frequency dependent conductivity region is called the a.c. region. The conducting mechanism can be explained based on the hoping mechanism model. According to this model, at higher frequency region the electrons are having lower relaxation time. Hence the electrons are back to its original lattice within a short time, which leads to the increase in the conductivity at higher frequency region. At low frequency region, the ions having enough time for back to its original site which leads to the d.c. conductivity [55]. Hence the total conductivity obtained can be calculated using the formula,

$$\sigma_{TOTAL} = \sigma_{AC}(\omega) + \sigma_{DC} \tag{12}$$

The $\sigma_{AC}(\omega)$ is the polarization conductivity which depends on the frequency as

$$\sigma_{AC}(\omega) = A(\omega)^s \tag{13}$$

Here A is the constant, ω is the angular frequency and s is an exponential power of frequency. Here $\sigma_{AC}(\omega)$ value increases with increasing frequency. The s value is obtained by taking slope of a.c. values from Fig. S3. The s value varies from 0.8 to 0.5 for 10–1000 ppm at room temperature. By using this s value, the coulomb well barrier of charge carriers (w_m) is calculated using the following equation,

$$s = 1 - \left\{\frac{6kT}{W_m}\right\} \tag{14}$$

$$w_m = \frac{6kT}{1-S} \tag{15}$$

The calculated value of w_m is found to decrease with increasing NH_3 concentration at room temperature. It shows that the barrier height decreases as the concentration increases (Fig. S4), which can be attributed to increase in the conductivity.

3.7. Gas response and selectivity

Further, the sensitivity of $MnFe_2O_4$ nanoparticles is calculated using the equation

$$\text{Gas Response} = \frac{Z''_{air} - Z''_{ammonia}}{Z''_{air}} \tag{16}$$

where Z''_{air} and $Z''_{ammonia}$ are the magnitudes of the imaginary impedance at the relaxation frequency in the impedance plots under air and ammonia atmosphere respectively [24]. The sensitivity is found to be an increasing with increasing concentration of ammonia and reaches a value of 99.8% whose values are shown in Fig. 6(a). Initially the sensitivity increases with increasing concentration of ammonia until 90 ppm. This may be due to the uniform distribution of smaller grains on the surface and the increased surface to volume ratio of these nanostructures. After 90 ppm the sensitivity reached a saturation, due to formation of multilayer on the pellet surface by ammonia vapor. This reduces the active site for interaction of ammonia molecules [55]. It is promising that the $MnFe_2O_4$ is having high sensitivity and can be able to detect even at low concentration of 10 ppm. It is lower than the Occupational Safety and Health Administration (OSHA) established level of ammonia (25 ppm).

The air around us has lot of chemical species in it. Hence the selectivity of the sample towards the particular gas becomes a key parameter in gas sensing applications. For testing the selectivity of the $MnFe_2O_4$ sample, vapors of different gases like chloroform, petrol and ethanol was introduced into the test chamber. The sensitivity was tested at two different concentrations namely 10 and 100 ppm which is shown in Fig. 6(b). The selectivity of the sample is in the order of Ammonia > Ethanol > Petrol > Chloroform. The selectivity towards ammonia at 10 ppm is 83.5%, whereas for ethenol, petrol and chloroform it is 68%, 2.4% and 0.68% respectively. Selectivity is found to increase for increasing value of concentrations.

4. Conclusion

$MnFe_2O_4$ was synthesised by the simple and cost effective polymer assisted combustion method. XRD analysis reveals the cubic structure and phase purity of $MnFe_2O_4$ sample without any impurity peaks. FTIR confirms the presence of functional groups. The FE-SEM images show that the particles had an average size of 30–35 nm. The saturation magnetization and coercivity of the sample was found using Vibrating Sample Magnetometer (VSM). The mesoporous nature of the sample was given by N_2 adsorption–desorption isotherm. Gas sensing properties are measured using the Impedimetric technique. It shows that both grain interior and grain boundary contribute to gas sensitivity at various concentrations. Further the resistance decreased with increasing concentration of ammonia indicating the n-type conduction mechanism of the sample. The sensor shows good sensitivity and selectivity towards ammonia. All these observations demonstrate the promise of using $MnFe_2O_4$ as ammonia gas sensor in the industrial and environmental monitoring.

Appendix A. Supplementary data

Supplementary data associated with this article can be found, in the online version, at http://dx.doi.org/10.1016/j.snb.2015.04.115

References

[1] G. korotcentov, Handbook of Gas Sensing Materials, Properties, Advantages and Shortcomings for Applications, vol. 1, Springer, 2013.
[2] B. Timmer, W. Olthuis, A.V.D. Berg, Ammonia sensor and their applications – a review, Sens. Actuators B 107 (2005) 666–677.
[3] G. Eranna, Metal Oxide Nanostructures as Gas Sensing Devices, Taylor and Francis Group, 2012.
[4] M.P. Massafera, S.I. Cordoba de Torresi, Evaluating the performance of polypyrole nanowires on the electrochemical sensing of ammonia in solution, J. Electroanal. Chem. 669 (2012) 90–94.
[5] D.V. Serebryakov, I.V. Morozov, A.A. Kosterev, V.S. Letokhov, Laser microphoto acoustic sensor of ammonia traces in the atmosphere, Quantum Electron. 40 (2010) 167–172.
[6] M. Vidotti, L.H. Dall'Antonia, S.I. Cordoba de Torresi, K. Bergamaski, F.C. Nart, Online mass spectrometric detection of ammonia oxidation products generated by polypyrrole based amperometric sensors, Anal. Chem. Acta 489 (2003) 207–214.
[7] E. Maciak, T. Pustelny, An optical ammonia gas sensing by means of Pd/CuPc interferometric nanostructures based on white light interferometry, Sens. Activators B 189 (2013) 230–239.
[8] M. Dziubaniuk, R.B. Koronska, J.S.J. Wyrwa, M. Rekas, Application of bismuth ferrite protonic conductor for ammonia gas detection, Sens. Activators B 188 (2013) 957–964.
[9] G.K. Mani, J.B.B. Rayappan, A highly selective ammonia gas sensor using spray deposited zinc oxide thin film, Sens. Activators B 183 (2013) 459–466.
[10] C. Nylander, M. Armgarth, I. Lundstrom, An ammonia detector based on a conducting polymer, Anal. Chem. Symp. Ser. 17 (1983) 203–207.
[11] P. Ivanov, J. Hubalek, A route toward more sensitive and less humidity sensitive screen printed SnO_2 and WO_3 gas sensitive layers, Sens. Actuatos B: Chem. 100 (2004) 221–227.
[12] J. Gong, Y. Li, Z. Hu, Z. Zhou, Y. Deng, Ultra sensitive NH_3 gas sensor from polyaniline nanograin enchased TiO_2 fibers, J. Phys. Chem. C 114 (2010) 9970–9974.
[13] H. Ma, K. Sun, Y. Li, X. Xu, Ultrasensitive chemoselective hydrogenation of chloronitrobenzenes chloroanilines over HCL acidified attapulgite-supported platinum catalyst with high activity, Catal. Commun. 10 (2009) 1363–1366.
[14] K. Shimizu, I. Chinzei, H. Nishiyama, S. Kakimoto, S. Sugaya, W. Matsutani, Satsuma, Doped vanadium oxides as sensing materials for high temperature operative selective ammonia gas sensors, Sens. Activators B 141 (2009) 410–416.
[15] P. Guo, H. Pan, Selectivity of Ti doped In_2O_3 ceramics as an ammonia sensor, Sens. Actuators B: Chem. 114 (2006) 762–767.
[16] N. Hu, Z. Yang, Y. Wang, L. Zhang, Y. Wang, X. Huang, H. Wei, Y. Zhang, Ultrafast and sensitive room temperature NH_3 gas sensors based on chemically reduced graphene oxides, Nanotechnology 25 (2014) 025502–025511.
[17] R.B. Kamble, V.L. Mathe, Nanocrystalline nickel ferrite thick film as an efficient gas sensor at room temperature, Sens. Actuators B 131 (2008) 205–209.
[18] Y.L. Liu, Z.M. Liu, Y. Yang, H.F. Yang, G.L. Shen, R.Q. Yu, Simple synthesis of $MgFe_2O_4$ nanoparticles as gas sensing materials, Sens. Actuators B 107 (2005) 600–604.
[19] S. Sam, A.S. Nesaraj, Preparation of $MnFe_2O_4$ nanoparticles by soft chemical routes, Int. J. Appl. Sci. Eng. 4 (2011) 223–239.
[20] L. Zhen, K. He, C.Y. Xu, W.Z. Shao, Synthesis and characterization of single crystalline $MnFe_2O_4$ nanorods via a surfactant free hydrothermal route, J. Magn. Magn. Mater. 320 (2008) 2672–2675.
[21] M. Siddique, N.M. Butt, Effect of particle size in the degree of inversion in ferrites investigated my mossbauer spectroscopy, Phys. B 405 (2010) 4211–4215.
[22] G. Balaji, N.S. Gajbhiye, G. Wilde, J. Weissmuller, Magnetic properties of $MnFe_2O_4$ nanoparticles, J. Magn. Magn. Mater. 242–245 (2002) 617–620.
[23] B. Sahoo, S.K. Sahu, S. Nayak, D. Dhara, P. Pramanik, Fabrication of magnetic mesoporous manganese ferrite nanocomposites as efficient catalyst for degradation of dye pollutants, Catal. Sci. Technol. 2 (2012) 1367–1374.
[24] P.K. Kannan, R. Saraswathi, An impedimetric ammonia sensor based on nanostructured α-Fe_2O_3, J. Mater. Chem. A 2 (2014) 394–401.
[25] M. Ahmed, E. Ateia, L.M. Salah, A.A. El-Gamal, Structural and electrical studies on La^{3+} substituted Ni-Zn ferrites, Mater. Chem. Phys. 92 (2005) 310–321.
[26] R.K. Bedi, I. Singh, Room temperature ammonia sensor based on cationic surfactant assisted nanocrystalline CuO, Appl. Mater. Interfaces 2 (2010) 1361–1368.
[27] S. Ounnunkad, Improving the magnetic properties of barium hexaferrites by La or Pr substitution, Solid State Commun. 138 (2006) 472–475.
[28] X.L. Liu, E.S.G. Choo, A.S. Ahmed, L.Y. Zhao, Y. Yang, R.V. Ramanujan, J.M. Xue, D.D. Fan, H.M. Fan, J. Ding, Magnetic nanoparticles loaded polymer nanospheres as magnetic hyperthermia agents, J. Mater. Chem. B 2 (2014) 120–128.
[29] K.H.J. Buschow, Handb. Magn. Mater. 8 (1995) 197–212.
[30] J.M.E. Loey, Noncollinear spin arrangement in ultrafine ferromagnetic crystallites, Phys. Rev. Lett. 27 (1971) 1140–1142.
[31] P. Guo, G. Zhang, J. Yu, H. Li, X.S. Zhao, Controlled synthesis, magnetic and photocatalitic properties of hollow spheres and colloidal nanocrystals of manganese ferrite, Colloids Surf. A: Phys. Chem. Eng. Aspects 395 (2012) 168–174.
[32] G.D.M. Muro, X. Battle, A. Labarta, Erasing the glassy state in magnetic fine particles, Phys. Rev. B 59 (1999) 13584–13587.
[33] S.E. Shirsath, R.H. Kadam, A.S. Gaikwad, A. Ghasemi, A. Morisako, Effect of sintering and the particle size on the structural and the magnetic properties of nanocrystalline $Li_{0.5}Fe_{2.5}O_4$, J. Magn. Magn. Mater. 323 (2011) 3104–3108.
[34] C. Liu, Z.J. Zhang, Size dependant superparamagnetic properties of Mn spinel ferrite nanoparticles synthesized from reverse micelles, Chem. Mater. 13 (2001) 2092–2096.
[35] J. Samuelsson, T. Undin, T. Fornstedt, Expanding the elution by characteristic point method for determination of various types of adsorption isotherms, J. Chromatogr. A 1218 (2011) 3737–3742.
[36] C. Nguyen, D.D. Do, A new method for the characterization of the porous materials, Langmuir 15 (1999) 3608–3615.
[37] Y. Lv, L. Gan, M. Liu, W. Xiong, Z. Xu, D. Zhu, D.S. Wright, A self template synthesis of hierarchial porous carbon foams based on banana peel for supercapacitor electrodes, J. Power Sources 209 (2012) 152–157.
[38] P. Khatri, B. Behera, R.N.P. Choudhary, Structural and impedance properties of $Ca_3Nb_2O_8$ ceramics, J. Phys. Chem. Solids 70 (2009) 385–389.
[39] W. Cao, Calculation of various relaxation times and conductivity for a single dielectric relaxation process, Solid State Ionics 42 (1990) 213–221.
[40] R. Gerhardt, Impedance and dielectric spectroscopy revisited: distinguishing localized relaxation from long-range conductivity, J. Phys. Chem. Solids 55 (1994) 1491–1506.
[41] M. Kumar, M. Anbu kulandainathan, I. Arulraj, R. Chandrasekaran, R. Pattabiraman, Electrical and sintering behavior of $Y_2Zr_2O_7$ (YZ) pyrochlore based materials—the influence of bismuth, Mater. Chem. Phys. 92 (2005) 295–302.
[42] P. Pattananuwat, M. Tagaya, T. Kobayashi, A novel highly sensitive humidity sensor based on poly(pyrrole-co-formyl pyrrole) copolymer film: AC and DC impedance analysis, Sens. Actuators B: Chem. 209 (2015) 186–193.
[43] C.K. Suman, K. Prasad, R.N. Chowdary, Complex impedance studies on tungsten-bronze electroceramic $Pb_2Bi_3LaTi_5O_{18}$, J. Mater. Sci. 41 (2006) 369–375.
[44] S. Shrabanee, R.N.P. Choudhary, Impedence studies of Sr modified $BaZr_{0.05}Ti_{0.95}O_3$ ceramics, Mater. Chem. Phys. 87 (2004) 256–263.
[45] S. Brahma, R.N.P. Choudhary, K.T. Awalendra, AC impedence analysis of $LaLiMo_2O_8$ electroceramics, Phys. B 355 (2005) 188–201.
[46] L. Satyanarayana, K.M. Reddy, S.V. Manorama, Nanosized spinel $NiFe_2O_4$: a novel material for the detection of liquefied petroleum gas in the air, Mater. Chem. Phys. 82 (2003) 21–26.
[47] B.C. Yadav, A. Yadav, S. Singh, K. Singh, Nanocrystalline zinc titanate synthesized via physicochemical route and its application as liquefied petroleum gas sensor, Sens. Actuators B 177 (2013) 605–611.
[48] S.K. Lee, D. Chang, S.W. Kim, Gas sensors based on carbon nanoflake/tin oxide composites for ammonia detection, J. Hazard. Mater. 268 (2014) 110–114.
[49] P. Guo, H. Pan, Selectivity of Ti-doped In_2O_3 ceramics as an ammonia sensor, Sens. Actuators B: Chem. 114 (2006) 762–768.
[50] C. Balamurugan, D.W. Lee, A selective NH_3 gas sensor based on mesoporous p-type NiV_2O_6 semiconducting nanorods synthesized using solution method, Sens. Actuators B: Chem. 192 (2014) 414–422.
[51] Z. Sun, L. Liu, D.Z. Jia, W. Pan, Simple synthesis of $CuFe_2O_4$ nanoparticles as gas sensing materials, Sens. Actuators B 125 (2007) 144–148.
[52] C.L. Hsu, K.C. Chen, T.J. Tsai, T.J. Hsueh, Fabrication of gas sensor based on p-type ZnO nanoparticles and n-type ZnO nanowires, Sens. Actuators B: Chem. 182 (2013) 190–196.
[53] N.S. Ramgir, Growth and gas sensing characteristics of p- and n-type ZnO nanostructures, Sens. Actuators B: Chem. 156 (2011) 875–880.
[54] V. Modafferi, G. Panzera, A. Donato, P.L. Antonucci, C. Chenille, N. Donato, D. Spadaro, G. Neri, Highly sensitive ammonia resistive sensor based on electrospun V_2O_5 fibers, Sens. Actuators B 163 (2012) 61–68.
[55] R. Pandeeswari, B.G. Jayaprakash, High sensing response of β-Ga_2O_4 thin film towards ammonia vapours: influencing factors at room temperature, Sens. Actuators B 195 (2014) 206–214.

Biographies

R. Hari Vignesh was born at Tamil Nadu, India in 1991. He did his bachelor's degree in physics at Nallamuthu Gounder Mahalingam (NGM) College, Tamil Nadu. He received his master's degree from Bharathiar University, Coimbatore, Tamil Nadu, India. Currently he is pursuing his PhD degree under guidance of Professor Y.S. Lee at School of Applied Chemical Engineering, Chonnam National University, Gwangju, South Korea. He works in the field of energy storage devices.

K. Vijaya Sankar received his M.Sc., degree in physics from Nallamuthu Gounder Mahalingam (NGM) College, Tamil Nadu in 2010. Subsequently, he obtained his M.Phil. degree in physics from Bharathiar University, Tamil Nadu. Presently he is pursuing Ph.D., degree under the supervision of Dr. R. Kalai Selvan, Assistant Professor, at Bharathiar University. His current research interest is synthesis of nanostructured ferrites and its ternary hybrid electrode composite for hybrid supercapacitor and sensor applications.

Samuthirapandian Amaresh completed his Ph.D. from Chonnam National University, South Korea under the guidance of Prof. Yun Sung Lee. He graduated from Anna University, Chennai (India) and did his Bachelors at Central Electrochemical Research Institute (CECRI), Karaikudi (India). He has authored and co-authored over 30 international publications. His research interest is to enhance the energy density of Li ion batteries and Supercapacitors with the help of electrode materials that store energy for various future applications like electric vehicles. His interest also includes the development of solid electrolytes for assembling high voltage and high energy all-solid-state lithium secondary batteries.

Yun-Sung Lee is currently working as an Associate Professor at Chonnam National University, Gwang-ju, in Korea. He received his M.S. from Chonbuk National University in 1998, and the research work was carried out under the guidance of Prof. Kee-Suk Nahm. He received Ph.D. in 2001 in applied chemistry from Saga University in Japan under the direction of Prof. Masaki Yoshio. He joined in 2001 as a Post-Doctoral Fellow as Doctoral Researcher with Professor Yuichi Sato, at Kanagawa University in Japan. He joined in 2003 at Chonnam National University as an Assistant Professor. He has authored and coauthored over 140 peer-reviewed international publications and is an active member of the lithium secondary battery field. His research interests are in the fields of Li-ion battery, electrode materials, and hybrid capacitor systems.

R. Kalai Selvan is currently working as Assistant Professor at Bharathiar University, Coimbatore, India. He received his both M.Sc. (physics) and M.Phil. (materials science) degrees from Madurai Kamaraj University in the year of 2000 and 2001, respectively. He received his Ph.D. in physics from Alagappa University, Karaikudi in 2006. Then he did his Post-Doctoral Research work at Bar-Ilan University, Israel under Prof. Aharon Gedanken for two years from January 2007 to December 2008. He joined in the Department of Physics as Lecturer in January 2009. He has authored and co-authored over 80 peer-reviewed international publications. His current research interest is in the fields of supercapacitors, Li-ion batteries, redox electrolytes and magnetic materials.